Korean J. Chem. Eng., 35(10), 2117-2126 (2018)
DOI: 10.1007/s11814-018-0115-8

pISSN: 0256-1115
eISSN: 1975-7220

Effect of cohesive powders on pressure fluctuation characteristics of a binary gas-solid fluidized bed

Liping Wei*,†, Youjun Lu, Jianbo Zhu*, Guodong Jiang*, Jun Hu*, and Haipeng Teng***

*School of Chemical Engineering, Northwest University, Xi'an, Shaanxi 710069, China
**State Key Laboratory of Multiphase Flow in Power Engineering (SKLMFPE),
Xi'an Jiaotong University, Xi'an, Shaanxi 710049, China
(*Received 22 January 2018 • accepted 30 June 2018*)

Abstract−The effect of cohesive particles on the pressure fluctuations was experimentally investigated in a binary gas-solid fluidized bed. The pressure fluctuation signals were measured by differential pressure sensors under conditions of various weight percentages of cohesive particles. The cohesive particles increased the fixed bed pressure drop per unit height and decreased the minimum fluidization velocity. The Wen & Yu equation well predicts the minimum fluidization velocity of the binary system. The addition of cohesive particles slightly decreased the bubble size in bubbling flow regime when the cohesive particles and the coarse particles mixed well, while the bubble size greatly decreased when the cohesive particles agglomerated on the bed surface. The time series of pressure fluctuations was analyzed by using the methods of time domain, frequency domain and wavelet transformation. The normalized standard deviation of pressure fluctuations decreased with increasing weight percentages of cohesive particles. A wide bandwidth frequency of 0 to 1 Hz got narrower with a single peak around 0.6 Hz with an increase in proportion of the cohesive particles. The meso-energy and micro-energy of pressure fluctuations were decreasing with increasing cohesive particles proportions, which indicated that adding cohesive particles could reduce the energy dissipation of bubble and particle fluctuations.

Keywords: Cohesive Particle, Pressure Fluctuations, Gas-solid Fluidized Bed, Single Bubble Regime, Meso-energy, Bubble Characteristics

INTRODUCITON

Fluidized bed reactors hve been widely used for coal pyrolysis, gasification and combustion [1,2]. The solid phase of the fluidized bed reactor is composed of multi-component particles with different properties. Take the coal pyrolysis fluidized bed reactor for example: the particles include inert heat storage particles, catalyst particles, raw coal, and char particles. These particles belong to Geldart A or B group particles, which are easily fluidized by the gas flow. However, some cohesive particles or Geldart C group particles will be produced during the reaction and flow processes due to the collision, abrasion, breakage and pyrolysis reaction. The cohesive particles affect the flow pattern and the hydrodynamics of the fluidized bed [3]. The bubble size and fraction tend to be reduced by adding less cohesive particles to a fluidized bed of coarse particles [4], while adding a large amount of cohesive powder is easy to agglomerate and form channeling because of their strong cohesivity [5].

Nakazato et al. [6] investigated bed expansion processes of a fluidized bed with binary particles of FCC (Geldart-A group) and $Al(OH)_3$ ($d_p \leq 15$ μm, Geldart-C group). They found the bed expansion height increases with increasing weight proportion of the cohesive particles in a range of 1 wt% to 5 wt%. An extended homogeneous bed expansion process was observed when adding small amount cohesive particles. Scuzzarella et al. [7] studied the effect of cohesive particles on the bed expansion of a binary gas-solid fluidized bed. The added cohesive particle was air pollution control residue, which was hard to be fluidized on its own. The fluidization quality and the voidage nonlinearly decreased with increasing amounts of the cohesive particles. Yates and Newton [8] validated that increasing cohesive particles increased the gas passing through the emulsion phase, which strengthened the conversion of the catalytic oxidative dehydrogenation of butene-1 in a fluidized bed. Han [9] added lighter and smaller particles into a binary particle system and observed smaller bubbles. Zou et al. [10] found the bubble size of cohesive particles is smaller than that for Geldart-A or Geldart-B group particles in a fluidized bed.

The cohesive particles have great effect on the bubble characteristics, bed expansion and reaction processes; thus it is necessary to reveal the physical mechanism and assess its impact. Pressure fluctuation signals provide a robust tool to evaluate the effect of the cohesive particles on the bubbling dynamics of binary mixtures in the gas-solid fluidized bed. The pressure fluctuation signals have been widely applied to identify different fluidization regimes, such as fixed bed, homogeneous, multiple bubbling, single bubbling, slugging, turbulent, fast fluidization and dilute transport bed, and forecast defluidization by agglomerate and bogging [11-15]. The characteristics of the pressure fluctuation signals in time domain and in frequency domain can be used to identify the multiple bubbling, single bubbling, and their transition. The amplitude of pressure fluctuation signals shows a trend of gradual decrease in the defluidiza-

†To whom correspondence should be addressed.
E-mail: weiliping@nwu.edu.cn

tion conditions [16]. Briens et al. [17] used a Kolmogorov-Smirnov test of the wavelet coefficient of pressure fluctuations to detect early logging induced by agglomerates of cohesive particle. Xiang et al. [18] found the amplitude, average value and Kolmogorov entropy of pressure fluctuations can determine the variation of superficial velocity, bed height and particle size. Davies et al. [19] found the pressure fluctuations standard deviation was not only linearly proportional to excess gas velocity, but also a clear function of particle size, which helped to the determine the particle size of binary mixture. This result indicated a potential method for early agglomerate detection. Although some investigations have been conducted to capture the pressure fluctuations characteristics of the binary gas solid fluidized bed, little attention has been paid to the effect of cohesive particles. It is still unclear how cohesive particles affect pressure fluctuation characteristics and the basic mechanism.

We experimentally studied the effects of cohesive particles on the bubbling and the pressure fluctuations. The pressure fluctuations under conditions of agglomerate and good mixing of the binary particles of cohesive particles and coarse particles were captured. The characteristics of the pressure fluctuations were analyzed in time domain, frequency domain and time-space analysis.

EXPERIMENTAL SET-UP

We investigated the effect of cohesive particles on the pressure fluctuations in a gas fluidized bed, as shown in Fig. 1. The pressured air is provided by a Roots blower and flows through pipes into the air chamber. A butterfly bumper and two ball valves are mounted on pipeline directly to regulate the air flow rate. The fluidized bed has a width of 200 mm, a height of 1,500 mm and a thickness of 15 mm, respectively. The air chamber has a height of 400 mm, which is long enough to filter the inlet air flow fluctuations and achieve a uniform air flow. A porous metals with a bore diameter of 30 μm is installed in the bottom of the fluidized bed to support the bed materials. Three differential pressure transducers (Baoji Institute of Sensor, China) are located 50 mm, 150 mm and 250 mm above the air distributer in the side wall. The measuring range of the differential pressure transducers is up to 5,000 Pa, and response time is less than 1 ms. The inlets of pressure joint pipes are coved by metal meshes with porosity diameter smaller than 30 μm to avoid the particles flowing into the measuring pipes.

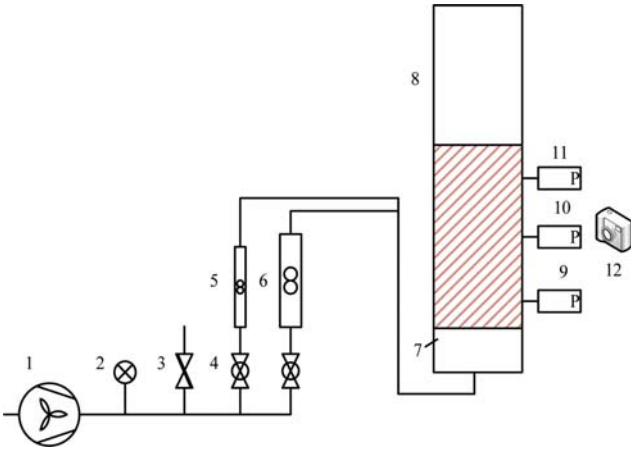

Fig. 1. Experimental system of gas-solid fluidized bed.

1. Roots blower
2. Pressure gage
3. Butterfly bamper
4. Ball valve
5. Float flow meter I
6. Float flow meter II
7. Air chamber
8. Fluidized bed
9. Differential pressure transducer 1 (DP1)
10. DP2
11. DP3
12. Camera

The sampling frequency of the DP signals is 1,000 Hz, with the number of samples being above 60000. The data acquisition system has a high sampling rate up to 200 kHz (NI CompactDAQ-8174). The analysis method of pressure fluctuation signals is illustrated in supplementary material, and the standard deviation, frequency information, wavelet transformation [20], R/S analysis and Hurst exponent [21] are obtained. Similar signals analysis methods were reported in our previous work for investigating the pressure fluctuations within a supercritical water fluidized bed [22]. A camera (50 frames per second) is applied to capture the cohesive agglomerate and bubble motion processes. The digital images of bubbling were shot by the camera, and the images were selected to implement binarization processing. The original images were converted into binary images with black (emulsion phase) and white color (bubble) as the work studied the bubble characteristics. The range of binarization threshold was between 0.31 and 0.35. Then, the images were denoised to reduce the experimental errors. Finally, the images were analyzed by a MATLAB code of flood fill method to capture the bubble diameter [23].

Table 1 lists the physical properties of the experimental materials. Quartz sand particles were used in experiment as fluidized materials, the equivalent volume diameter of particles were 0.3 mm-0.5 mm and the density was 2,650 $kg \cdot cm^{-3}$. The cohesive particle was corn powder with diameter 3 μm-25 μm and real density of 750-780 $kg \cdot m^{-3}$. The uncertainty of experimental data was analyzed. The uncertainty of differential pressure, and flow rate are less than 0.25% and 0.2%, respectively.

RESULTS AND DISCUSSION

1. Effects of Cohesive Particles on Time Averaged Pressure Drop

Fig. 2 shows the effects of cohesive particles on pressure drop. The plot of pressure drop vs. superficial velocity is similar to each other whether adding the cohesive particles or not. The increased superficial velocity increases the pressure drop in the fixed bed, while the pressure drop increases no more when particles are fully fluidized. All plots in Fig. 2 have turning points at the minimum fluidization velocities. Initially, the cohesive particles and the sand were separated. The sand was set on the bottom of the fluidized bed and the cohesive powder was set above the height of the sand. When the superficial velocity is low, the air passes through the fixed

Table 1. Physical properties of the experimental materials

Parameter	Sand	Cohesive powder (corn powder)
Density ($kg \cdot m^{-3}$)	2650	750-780
Diameter range (mm)	0.3-0.5	0.003-0.025

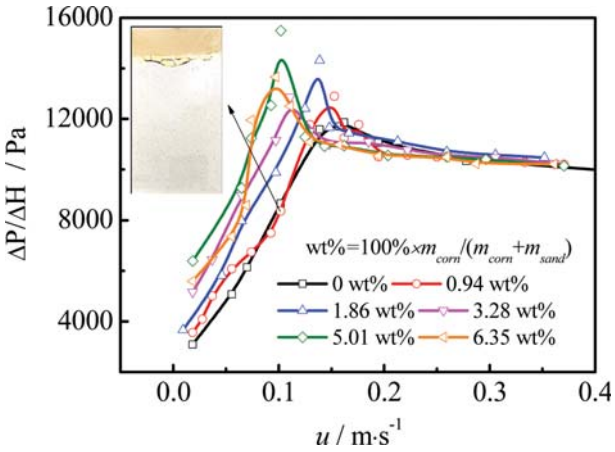

Fig. 2. Effects of cohesive particles on pressure drop.

sand and the fixed cohesive powders. In the situation, the air hardly flows across the space between two cohesive particles due to large flow resistance within the agglomeration. The air flow is through the space between agglomeration clumps. The fixed bed pressure drop increases with an increase in the proportion of the cohesive particles varying from 0 wt% to 5.01 wt%, while the pressure drop is reduced when the cohesive particles proportion increases to 6.35 wt%. The relationships between the fixed bed pressure drop and the proportion of the cohesive particles are nonlinear. On the whole, adding cohesive particles induces a larger pressure drop in fixed bed. The increased bed resistance is mainly attributed to the cohesive force between the cohesive particles, which requires a larger pressure drop to balance. When the sand and cohesive particle agglomeration were initially fluidized, the size of agglomeration decreased and interaction between sand and the agglomeration increased, which promoted the mixing of the binary particles. Accordingly, the bed pressure drop was reduced in this process. When the binary particles were fully fluidized, the pressure drop showed a close trend to each other because the effective weights of the bed materials were close to each other. The interaction between coarse particles and the agglomerates further promoted the mixing of the cohesive particles and the coarse particles, and increased the distance between cohesive particles, which weakened the influence of the cohesive force. The cohesive particle increases the bed resistance of fixed bed, while the effect of the cohesive particle on the pressure drop of fluidized bed is not remarkable.

Table 2. Minimum fluidization velocity equations

Author	Equations	Parameters
Wen and Yu [24]	$Ar = 24.5Re_{mf}^2 + 1650Re_{mf}$	$Ar = \frac{\bar{d}^3 \rho_g (\bar{\rho} - \rho_g) g}{\mu^2}$ $Re_{mf} = \frac{\bar{d} \rho_g u_{mf}}{\mu}$
Noda et al. [25]	$Ar = 36.2\left(\frac{d_p \rho_p}{d_c \rho_c}\right)^{-0.196} Re_{mf}^2 + 1397\left(\frac{d_p \rho_p}{d_c \rho_c}\right)^{0.296} Re_{mf}$	$\frac{1}{\bar{\rho}} = \frac{w_c}{\rho_c} + \frac{w_p}{\rho_p}$ $\frac{1}{\bar{d}\bar{\rho}} = \frac{w_c}{d_c \rho_c} + \frac{w_p}{d_p \rho_p}$

Fig. 3 shows the variation of minimum fluidization velocity with an increase in cohesive particles. The minimum fluidization velocity decreases with the increasing cohesive particle. We used the Wen and Yu correlation [24] and Noda correlation [25] to calculate the minimum fluidization velocity based on the mass-weighted density and diameter. Table 2 shows the equations. The results show both two correlations can predict the same variation trends. The minimum fluidization velocity calculated by the Wen and Yu correlation is much closer to the experimental results than Noda correlation. The maximum prediction error of the Wen and Yu correlation is 23%.

2. Effects of Cohesive Particles on Bubbling

Fig. 4 shows the variation of bubble diameter along the bed height. When the cohesive particle proportion is 0 wt%, the bubble size increase from 4 cm to 7 cm with the increasing bed height. However, the bubble size significantly reduces and fluctuates around 2 cm when the bed surface agglomeration is formed by adding 0.94 wt% cohesive powder. The binary particles are well mixed in other conditions of 1.86 wt%-6.35 wt%. In these conditions, the bubble diameter first increases and then decreases along the bed height, and the trend of which is similar to the condition without cohesive particles. However, the bubble diameter of the binary particle sys-

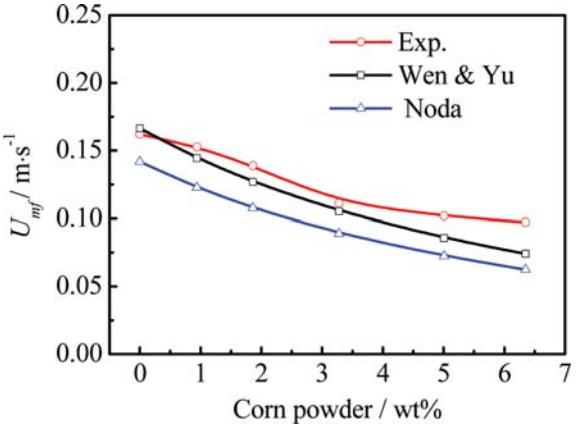

Fig. 3. Effects of cohesive particles on minimum fluidization velocity.

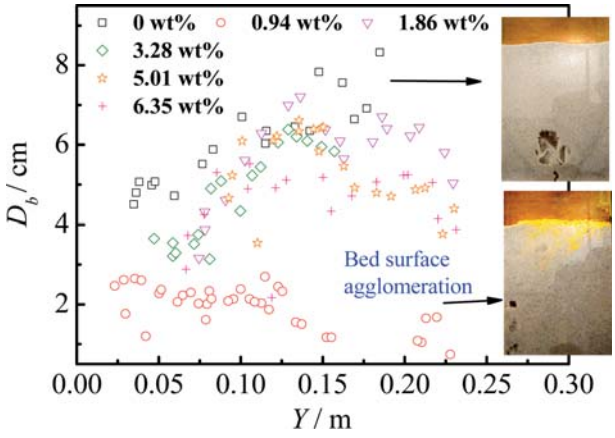

Fig. 4. The influence of cohesive particles on bubble diameter.

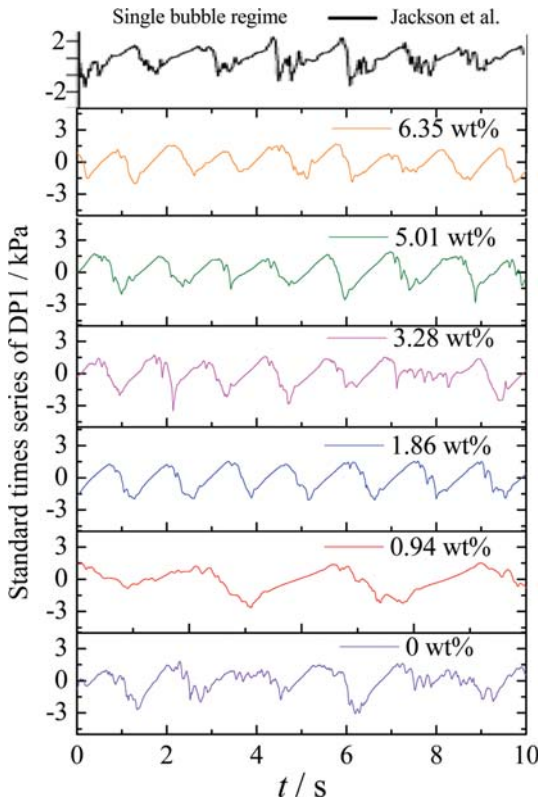

Fig. 5. The pressure time series obtained in different cohesive particle proportions (u_f=18.51 cm·s^{-1}).

tem is lower than that of the monodisperse sand particle system. The added cohesive particles without forming agglomerate will reduce the bubble size and put more gas passing through the emulsion phase.

3. Effects of Cohesive Particles on Pressure Deviation

The pressure fluctuations can be applied to determine the flow regimes. Fig. 5 compares the pressure time series measured in this work with that obtained by Jackson et al. [13] under the condition of 0 wt% cohesive particle. A clear periodicity of the pressure fluctuations is observed in the figure, which indicates a single bubble regime. The amplitude of pressure fluctuations does not change with an increase in cohesive particle proportion. The time between two peaks of pressure fluctuations is delayed when the bed surface agglomerates are formed in the condition of cohesive particle proportion of 0.94 wt%, and shortened when the binary particles are well mixed in the cohesive particle proportion range of 1.86 wt%-6.35 wt%. This result indicates that the agglomerate on the bed surface slowed down the bubbling frequency.

Standard deviations were normalized with respect to the standard deviation at maximum value. Fig. 6 shows the effects of cohesive particles on the normalized standard deviations. The standard deviation of pressure fluctuation is proportional to excess gas velocity when the cohesive particle proportion is 0 wt%. A linear relationship between the standard deviation and excess gas velocity was explained by Puncochar and Drahos with an energy dissipation model [26]. Other researchers reported a nonlinear relationship between the standard deviation and excess gas velocity in

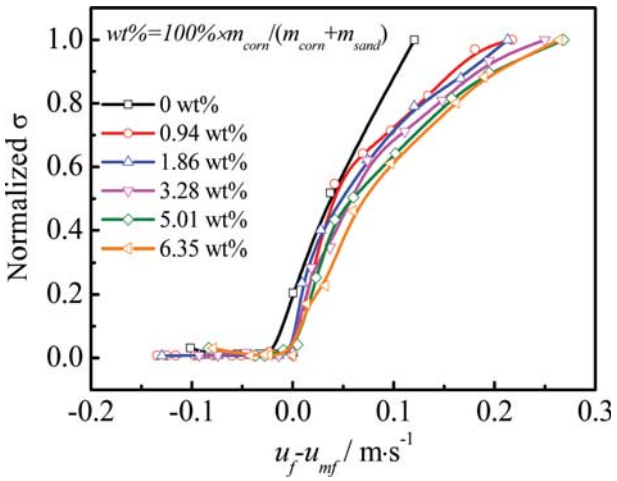

Fig. 6. Effects of cohesive particles on normalized standard deviation.

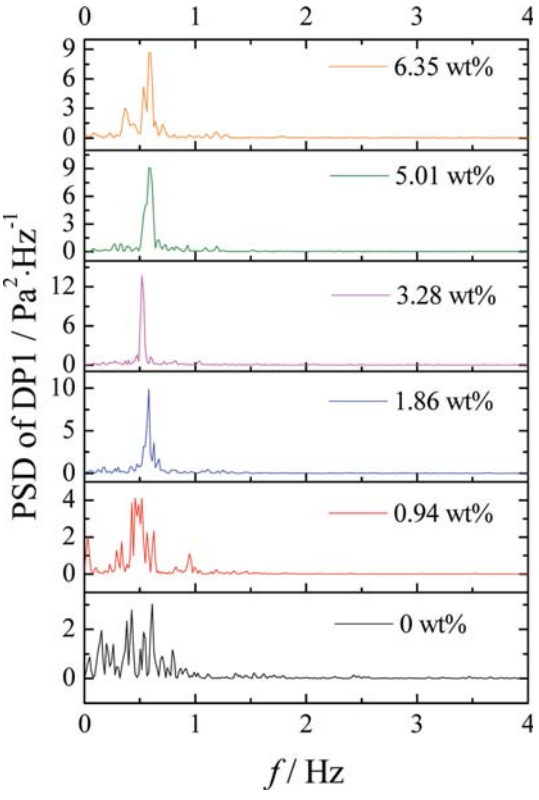

Fig. 7. Effects of cohesive particles on the PSD of DP signals (u_f= 18.51 cm·s^{-1}).

high superficial velocity regime [27,28]. In Fig. 6, a linear relationship between normalized standard deviation and excess gas velocity is changed by adding cohesive particles, and the more cohesive particles put in, the lower normalized standard deviation is. The results indicate that the cohesive particles reduce the energy dissipation of the binary particles system. The standard deviation is considered a proportion function, which is shown below [26].

$$\sigma \approx (1-\varepsilon_{mf})(\rho_s-\rho_f)g(u_f-u_{mf}) \quad (1)$$

For a binary particle system, the solid density of mixture is reduced with an increase in cohesive particle proportion, which decreases the differential density between solid and gas and then decreases the value of standard deviation.

4. Effects of Cohesive Particles on Power Density Spectrum

Note that the experimental data at variable superficial gas velocities from different data runs were analyzed and nearly the same results were obtained. To simplify, the results at u_f=18.51 cm·s^{-1} were taken as an example to illustrate in the following discussion. The results are of universal significance in the single bubble flow regime for the binary particles. From Fig. 7, the PSD of DP1 shows a wide bandwidth frequency of 0 to 1 Hz without adding the cohesive particles. However, with an increase in the proportion of cohesive particles, the bandwidth frequency becomes narrower, and single peaks are observed when the proportion is equal and above 1.86 wt%. In common, the frequency of the pressure fluctuations reflects the bubbling frequency in the gas solid fluidized bed. The cohesive particles do not significantly change the main bubbling frequency, while it reduces bubble fluctuations. The cohesive particles have lubrication effects on the interface between the emulsion phase and bubble, which will reduce the flow resistance force suffered by the bubble from the emulsion phase. Also, the cohesive particles reduce the gas flow resistance in the emulsion phase by reducing the collision frequency between the coarse particles.

5. Effects of Cohesive Particles on Multiscale Energy

To investigate the effects of the cohesive particle on the fluid dynamics behavior of the binary particles fluidized bed, wavelet transform and R/S analysis were applied to decompose the pressure fluctuation signals to macro-scale, meso-scale and micro-scale. Table 3 shows decomposition errors of fluctuations using different Daubechies wavelets at u_f=18.51 cm·s^{-1} for nine level without cohesive particles. Obviously, the Daubechies wavelet (db2) has minimum decomposition error. In literature, db2 is also suggested to decomposing the pressure fluctuations in a gas-solid or liquid-solid fluidized bed [29,30]. This work calculates the Shannon entropy at different decomposition levels. Shannon entropy did not decrease until the decomposition levels after nine. Thus db2 and nine level were used in present work to obtain detailed and approximation decomposed signals. The decomposed signals at u_f=18.51 cm·s^{-1} for variable cohesive particle proportion are drawn in Fig. 8.

Table 3. Decomposition errors of fluctuations using different Daubechies wavelets at u_f=18.51 cm·s^{-1} for nine level without cohesive particles

D2	D3	D4	D5	D6	D7	D8	D9	D10
2.15775E-06	4.0168e-05	7.2759e-06	1.1031e-05	5.4252e-06	7.1665e-06	1.7320e-05	1.0161e-04	1.5257e-05

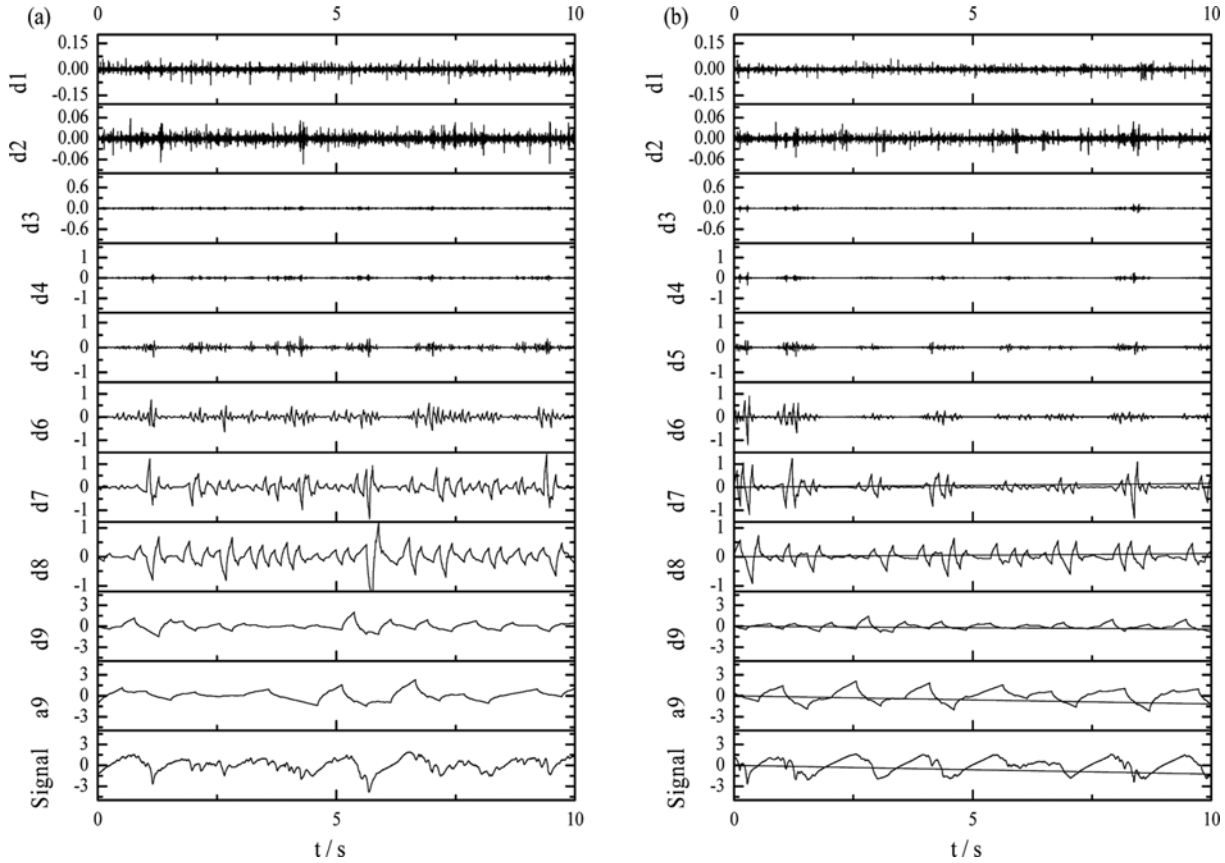

Fig. 8. Nine levels of each detail and approximation decomposed signal by the second-order Daubechies mother wavelet u_f=18.51 cm·s^{-1}, (a) 0 wt%; (b) 0.94 wt%; (c) 1.86 wt%; (d) 3.28 wt%; (e) 5.01 wt%; (f) 6.35 wt%.

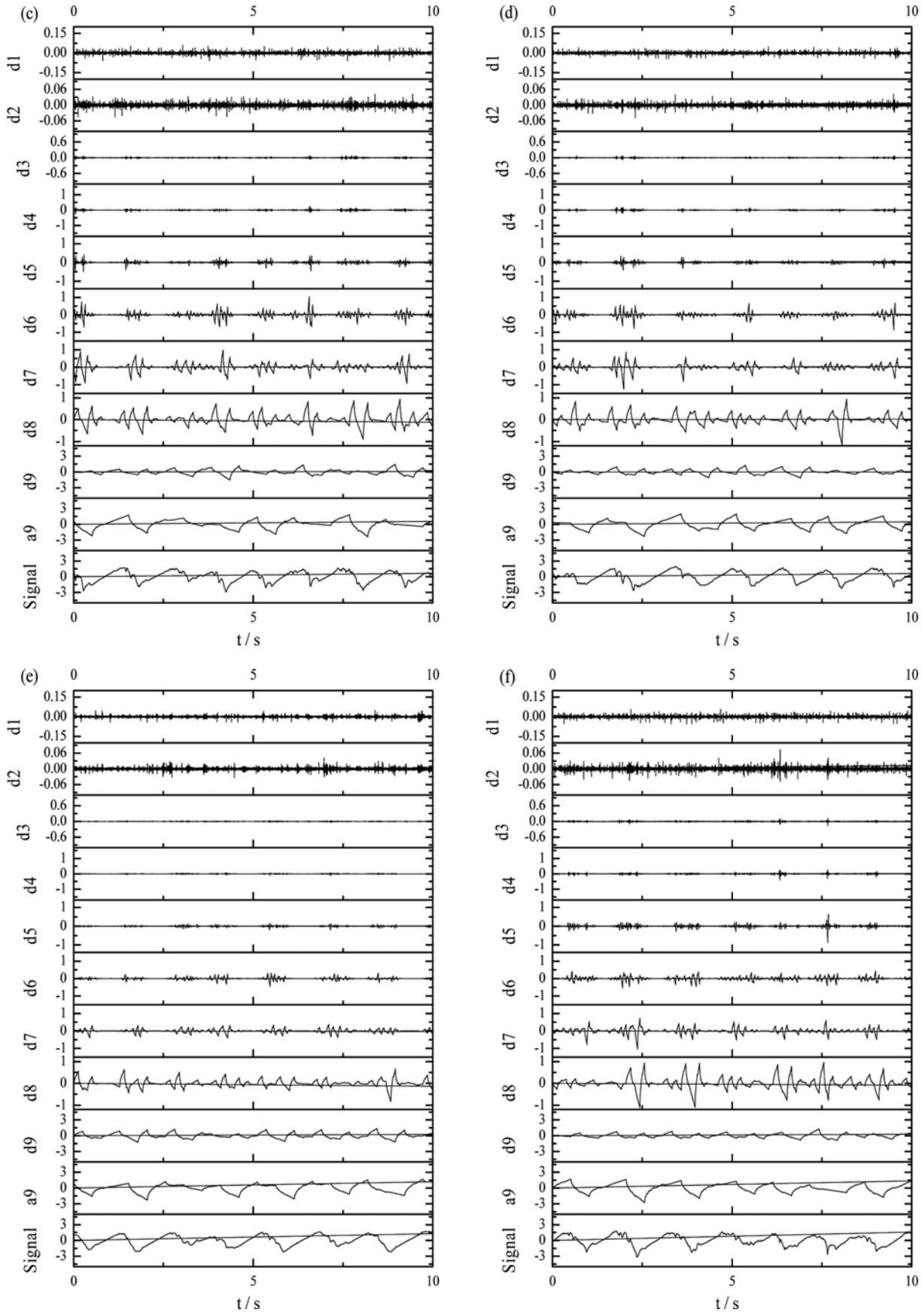

Fig. 8. Continued.

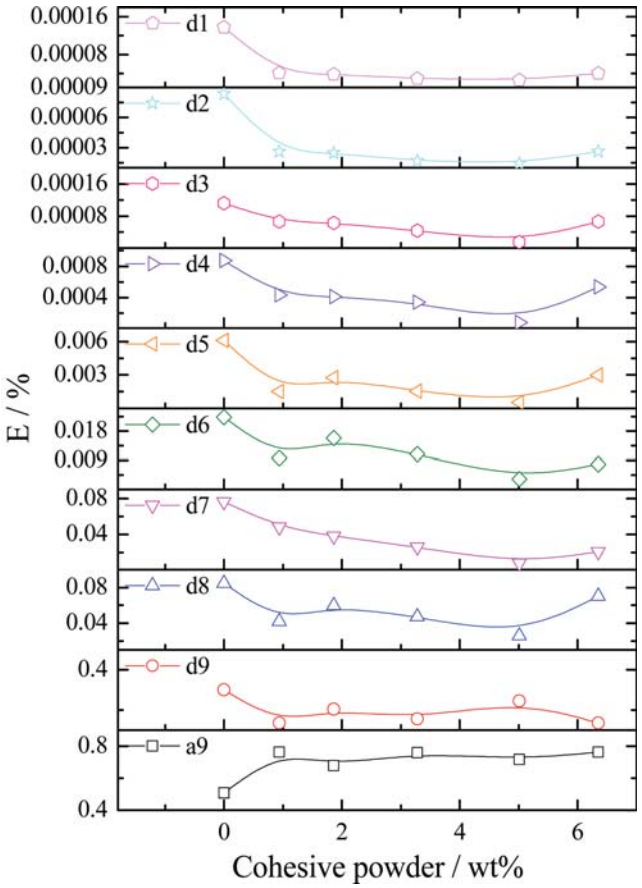

Fig. 9. Effects of cohesive powder on the sub-signal energy properties (u_f=18.51 cm·s^{-1}).

Fig. 9 shows the variations of decomposition energy proportion of low-frequency sub-signal a9, and high-frequency sub-signal d1-d9 with increasing cohesive particles. The energy proportion of approximation sub-signal a9 is the highest, which indicates the macro-scale dynamics of bubbling is dominant in the single bubble regime. The energy proportions of high-frequency sub-signal d1-d9 are much lower than that of sub-signal a9. The energy proportion of approximation sub-signal a9 increases with an increase in cohesive particle proportion in the conditions investigated in this work. The energy proportion of high-frequency sub-signal d9 increases in the range of 0.94 wt%-5.01 wt%, and then decreases when the cohesive particle proportion reaches 6.35 wt%. The variation trends of energy proportion of high-frequency sub-signal d1-d8 with the cohesive particle proportion are just opposite to that of sub-signal d9. Thus, adding cohesive particle will increase the macro-scale fluctuations and reduce the micro-scale fluctuations and micro-scale energy dissipation.

We analyzed the R/S of nine levels of a multi-resolution decomposed signals in Fig. 10. Hurst exponent can be achieved by the linear regression of Log[Ep(R/S)] vs. log(n). There is only one Hurst exponent corresponding to the linear relationship of Log[Ep(R/S)] vs. log(n) for the decomposed level 1 and 2 detail signals. The value of Hurst exponents of level 1 and 2 signals is lower than 0.5, which indicates an anti-persistent dynamic behavior in the binary gas-solid fluidized bed. Considering low Hurst exponents refer to random or less persistent, these sub-signals of level 1 and 2 correspond to microscale stochastic flow structure [30,31]. The stochastic flow structure includes the microscale interaction between particles and fluid or the interaction between particles, because the particles move randomly within the fluidized bed even in a small space. The detailed signals of level 1 and level 2 represent the high frequency of the original signals, which also reflects a high frequency flow behavior of the particle-particle interaction and the particle-fluid interaction. However, the decomposed 3-9-level detail signals have two distinct Hurst exponents. One Hurst exponent is close to one at smaller n, and the other is smaller than 0.5 at larger n, which indicates a bifractal flow structure. Bai et al. [32] think the bifractal structure was characterized by two Hurst exponents and characterize the motions of the emulsion phases and bubbles in the fluidized bed. The bubble motion shows a high persistent dynamic feature, which refers to the Hurst exponents at smaller n. The emulsion phase motion shows a highly anti-persistent dynamic feature, which induced the Hurst exponent at larger n. The level 9 sub-signal has only one high Hurst exponent, which reflects the macroscale interaction of the bed. The Hurst exponent characteristics of the decomposed signals are similar for variable conditions

Table 4. Hurst exponent of multi-resolution sub-signals at u_f=18.51 cm·s^{-1}

	d1	d2	d3	d4	d5	d6	d7	d8	d9	a9
0 wt%	-	-	0.985	0.986	0.988	0.999	0.989	0.999	0.998	0.998
	0.298	0.365	0.125	0.305	0.307	0.318	0.257	0.372	0.298	-
0.94 wt%	-	-	0.985	0.985	0.989	0.979	0.988	0.986	0.999	0.997
	0.297	0.313	0.115	0.310	0.370	0.321	0.244	0.322	0.288	-
1.56 wt%	-	-	0.995	0.988	0.987	0.979	0.990	0.992	0.999	0.996
	0.295	0.334	0.120	0.325	0.357	0.308	0.286	0.327	0.277	-
3.28 wt%	-	-	0.984	0.988	0.990	0.995	0.986	0.909	0.991	0.998
	0.208	0.385	0.135	0.322	0.377	0.388	0.255	0.365	0.299	-
5.01 wt%	-	-	0.905	0.996	0.998	0.989	0.986	0.997	0.998	0.995
	0.306	0.312	0.145	0.335	0.355	0.365	0.258	0.390	0.221	-
6.35 wt%	-	-	0.998	0.989	0.986	0.987	0.988	0.999	0.996	0.998
	0.313	0.311	0.135	0.368	0.367	0.378	0.297	0.302	0.288	-

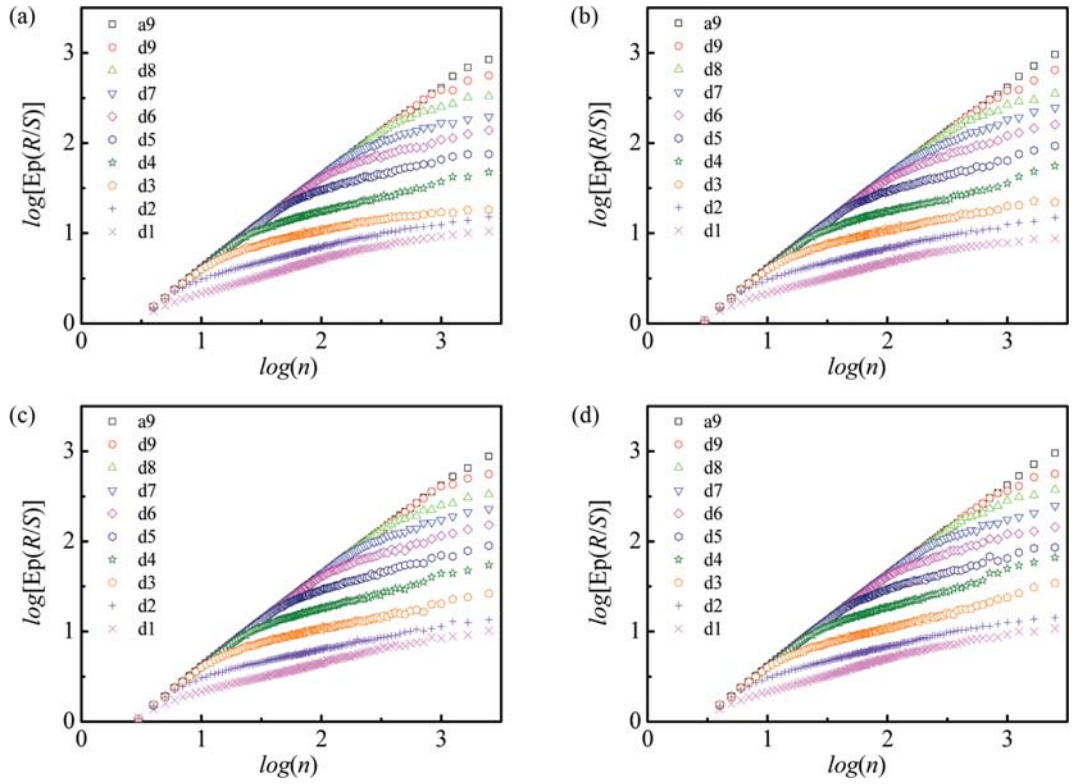

Fig. 10. R/S analysis of nine levels of a multi-resolution decomposed signals u_f=18.51 cm·s^{-1}, (a) 0 wt %; (b) 1.86 wt%; (c) 5.01 wt%; (d) 6.35 wt%.

of different cohesive powder proportions. This result indicates that the addition of the cohesive particle did not change the basic bubbling flow regime.

Table 4 lists the Hurst exponent of multi-resolution sub-signals at u_f=18.51 cm·s^{-1}. Based on the analysis of the Hurst exponents, the sub-signals can be divided into three categories: micro-scale signals (sub-signals of d1 and d2 with Hurst exponents below 0.5), meso-scale signals (sub-signals of d3-d9 with one Hurst exponents below 0.5 and the other above 0.5), and macro-scale signals (approximation sub-signal of a9 with a Hurst exponent approaching 1). For a bubbling fluidized bed, the macro-scale signals reflect the motion of the whole bed and the interaction between bed and wall, and the meso-scale signals are related to the motion of bubbles, and the interaction between emulsion phase and bubbles, and micro-scale signals corresponds to fluctuations of individual particles and the interactions between particles and gas in the bubble phase or emulsion phase.

Fig. 11 further investigates the effect of the cohesive particles on the energy of macro-scale, meso-scale and micro-scale decomposed signals at variable conditions. The energy of macro-scale signals and meso-scale signals is close to each other at u_f=18.51 cm·s^{-1} without the effect of cohesive particle, which indicates a strong meso-scale interaction of bubble and the emulsion phase. However, adding cohesive particles greatly increased the energy of macro-scale signals from 50% to 76%, decreased the meso-scale energy proportion form 49% to 23%, and sharply reduced the micro-scale energy proportion. Zhao and Yang [30] found the energy proportion of meso-scale signals was up to 95% in a typical multi-bubble

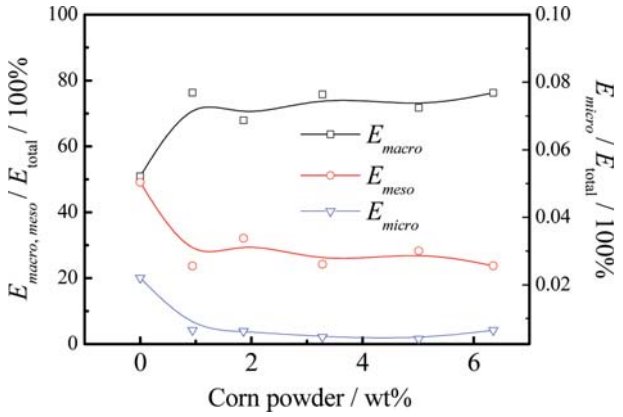

Fig. 11. Effects of cohesive particles on the meso-energy of pressure fluctuations (u_f=18.51 cm·s^{-1}).

gas solid fluidized bed. Wei et al. [22] found the macro scale energy is dominant in an SCW fluidized bed, which is a quasi-homogeneous expansion system with large number of small bubbles. Skeikhi et al. [29] also observed the highest energy proportion of macro scale signals in a homogeneous liquid solid system. Therefore, the bubbling gas-solid fluidized bed, a heterogeneous system, tends to be a quasi-homogeneous system under the effect of the cohesive particles. This result is consistent with that the added cohesive particles reduce the bubble size. The cohesive particles play an important role of reducing the fluctuations of bubbles and particles during their moving. A remarkable effect of the cohesive

particles on the flow can be achieved by adding even little mount of cohesive particles.

CONCLUSION

The pressure fluctuation signals of a binary fluidized bed were measured, and the effect of the cohesive particles on the pressure fluctuation characteristics was studied by applying signals analysis of time domain, frequency domain and wavelet transform. Based on the experimental investigations, the following conclusions can be drawn:

(1) Adding cohesive particles increased the bed pressure drop of fixed bed; the minimum fluidization of the binary particles with cohesive particles could be predicted by the Wen and Yu equation.

(2) The bubble size did not increase with the increasing bed height, and the diameter fluctuated around 2 cm when agglomerate formed on the bed surface. The variation trend of bubble diameter along the bed height was similar to that without cohesive particles, while the bubble diameter decreased with an increase in weight percentage of the cohesive particles.

(3) The peak of pressure fluctuations was delayed when the cohesive powders agglomerated on bed surface, and shortened when the binary particles were well mixed. Adding cohesive particle decreased the normalized standard deviation of the pressure fluctuations.

(4) The bandwidth frequency of the gas solid fluidized bed became narrower and even showed single peak when the cohesive particle proportion was in the range of 0.94 wt%-6.35 wt%.

(5) Adding cohesive particles increased the energy of macro-scale signals, decreased the meso-scale energy proportion and the micro-scale energy proportion. The fluctuations induced by bubbles and particles were greatly reduced by even mixing the coarse particle with a little mount of the cohesive particles.

ACKNOWLEDGEMENT

This work is currently supported by the National Natural Science Foundation of China through contract No. 51606153 and 91634109, Natural Science Basic Research Plan in Shaanxi Province of China (No. 2016JQ5101), and Project funded by China Postdoctoral Science Foundation (2017M613189).

NOMENCLATURE

Ar : Archimedes number
$\overline{d}$: mass-weighted diameter [m]
d_c : cohesive particle diameter [m]
d_p : coarse particle diameter [m]
d_h : bubble diameter [m]
E : energy proportion
g : gravitational acceleration [m·s^{-2}]
Y : bed height [m]
N : length of time series
n : index function
ΔP : pressure drop [Pa]
Re : Reynolds number
x(n) : time series of fluctuation signals
$\overline{x}$: mean value
u : superficial fluid velocity [m·s^{-1}]

Greek Letters

ε : voidage
μ : viscosity [Pa·s]
ρ : density [kg·m^{-3}]
σ : normalized standard deviation

Subscripts

c : cohesive particle
f : fluid
mf : minimum fluidization
marco : macroscopic
micro : microscopic
meso : mesoscopic
p : coarse particle
total : total energy

Abbreviation

DP : difference pressure

SUPPORTING INFORMATION

Additional information as noted in the text. This information is available via the Internet at http://www.springer.com/chemistry/journal/11814.

REFERENCES

1. Z. A. B. Z. Alauddin, P. Lahijani, M. Mohammadi and A. R. Mohamed, *Renew. Sust. Energy Rev.*, **14**, 2852 (2010).
2. R. C. Borah, P. Ghosh and P. G. Rao, *Int. J. Energy Res.*, **35**, 929 (2011).
3. J. Li, T. Nakazato and K. Kato, *Chem. Eng. Sci.*, **59**, 2777 (2004).
4. Z. Yang, Y. Tung and M. Kwauk, *Chem. Eng. Commun.*, **39**, 217 (1985).
5. H. O. Konon, C. C. Huang, E. Morimoto, T. Nakayama and T. Hikosaka, *Powder Technol.*, **53**, 163 (1987).
6. T. Nakazato, Y. Suzuki, E. A. Mahmoud and N. Nakagawa, *Effect of size and hold-up of cohesive fine powders on particulate fluidization of binary powder-particle mixtures*, Asian Pac. Confederation Chem. Eng. Congress Progr. Abstracts (2004), DOI:10.11491/apcche.2004.0.40.0.
7. A. Scuzzarella, M. F. Bertos, S. J. Simons, C. D. Hills and P. J. Carey, *Powder Technol.*, **163**, 18 (2006).
8. J. G. Yates and D. Newton, *Chem. Eng. Sci.*, **41**, 801 (1986).
9. B. Han, *Bubble dynamics and bed expansion for single-component and binary gas-solid fluidization systems*, The University of Western Ontario (2017).
10. Z. Zou, H. Z. Li and Q. S. Zhu, *Powder Technol.*, **212**, 258 (2011).
11. H. Bi, J. Grace and J. Zhu, *Powder Technol.*, **82**, 239 (1995).
12. H. Bi, *Chem. Eng. Sci.*, **62**, 3473 (2007).
13. F. Johnsson, R. C. Zijerveld, J. C. Schouten, C. M. van den Bleek and B. Leckner, *Int. J. Multiphase Flow*, **26**, 663 (2000).

14. J. Gómez-Hernández, D. Serrano, A. Soria-Verdugo and S. Sánchez-Delgado, *Chem. Eng. J.*, **284**, 640 (2016).
15. J. van Ommen, S. Sasic, J. Van der Schaaf, S. Gheorghiu, F. Johnsson and M. Coppens, *Int. J. Multiphase Flow*, **37**, 403 (2011).
16. G. Tardos and R. Pfeffer, *Powder Technol.*, **85**, 29 (1995).
17. C. Briens, M. Hamidi, F. Berruti and J. Mcmillan, *Powder Technol.*, **316**, 92 (2017).
18. J. Xiang, Q. Li, Z. Tan and Y. Zhang, *Chem. Eng. Sci.*, **174**, 93 (2017).
19. C. E. Davies, A. Carroll and R. Flemmer. *Powder Technol.*, **180**, 307 (2008).
20. J. Di, *The wavelet analysis theory*, Science Press, Beijing (2010).
21. H. E. Hurst, *Trans. Am. Soc. Civil Engineers*, **116**, 776 (1951).
22. L. P. Wei and Y. J. Lu, *Chem. Eng. Res. Design*, **109**, 657 (2016).
23. Y. Lu, J. Huang and P. Zheng, *Chem. Eng. J.*, **274**, 123 (2015).
24. C. Wen and Y. Yu, Mechanics of fluidization, *Chem. Eng. Prog. Symp. Ser.*, **62**, 100 (1966).
25. K. Noda, S. Uchida, T. Makino and H. Kamo, *Powder Technol.*, **46**, 149 (1986).
26. M. Puncochar and J. Drahos, *Chem. Eng. Sci.*, **60**, 1193 (2005).
27. Y. O. Chong, D. P. O'Dea, E. T. White, P. L. Lee and L. S. Leung, *Powder Technol.*, **53**, 237 (1987).
28. S. C. Hong, B. R. Jo, D. S. Doh and C. S. Choi, *Powder Technol.*, **60**, 215 (1990).
29. A. Sheikhi, R. Sotudeh-Gharebagh, N. Mostoufi and R. Zarghami, *Powder Technol.*, **235**, 787 (2013).
30. G. B. Zhao and Y. R. Yang, *AIChE J.*, **49**, 869 (2003).
31. A. I. Karamavruç and N. N. Clark, *Powder Technol.*, **90**, 235 (1997).
32. D. Bai, A. S. Issangya and J. R. Grace, *Ind. Eng. Chem. Res.*, **38**, 803 (1999).

Supporting Information

Effect of cohesive powders on pressure fluctuation characteristics of a binary gas-solid fluidized bed

Liping Wei*,†, Youjun Lu, Jianbo Zhu*, Guodong Jiang*, Jun Hu*, and Haipeng Teng***

*School of Chemical Engineering, Northwest University, Xi'an, Shaanxi 710069, China
**State Key Laboratory of Multiphase Flow in Power Engineering (SKLMFPE),
Xi'an Jiaotong University, Xi'an, Shaanxi 710049, China
(*Received 22 January 2018 • accepted 30 June 2018*)

Analysis method of the pressure fluctuations

Standard deviation of signal series, x(n), is always used to express the amplitude for time domain analysis. The standard deviation is the square root of second-order statistical moment:

$$\sigma=\sqrt{\frac{1}{N-1}\sum_{n=1}^{N}[x(n)-\bar{x}]^2} \tag{1}$$

where $\bar{x}$ is the average of x(n):

$$\bar{x}=\frac{1}{N-1}\sum_{n=1}^{N}x(n) \tag{2}$$

Frequency domain information can be obtained by Fourier transform, which requres steady signals with sufficient statistical significance. However, the typical samples in fluidized bed are finite, which leads to a large variance of power spectrum. Welch's method has been used to decrease the variance. The time series is divided into L segments of individual length N_s, which are represented as:

$$x_i(n)=x(n+iN_s);\ n=1, 2, 3, ---, N_s;\ i=1, 2, 3, ---, L \tag{3}$$

The power spectrum estimate of each segment by Fourier transform with a window function w(n) is:

$$P_{xx}^{i}(f)=\frac{1}{\Sigma_{n=1}^{N_s}w^2(n)}\left[\sum_{n=1}^{N_s}x_i(n)w(n)e^{-j2\pi nf}\right]^2 \tag{4}$$

The averaged power spectrum is:

$$P_{xx}(f)=\frac{1}{L}\sum_{i=1}^{L}P_{xx}^{i}(f) \tag{5}$$

A Hanning window is used as window function, w(n). This window is a smooth one with a continuous first derivative, and both the window and its derivative are zero at the endpoints.

In order to obtain unsteady amplitude and impulse signals, wavelet transform is applied to analyzed the high possible time-frequency resolution:

$$CWf(m, o)=\langle f, \zeta_{m,o}\rangle=\frac{1}{|m|^{1/2}}\int x(n)\zeta^{*}\left(\frac{t-o}{m}\right)dt \tag{6}$$

In Eq. (6), ζ is mother wavelet function, which is a prototype for producing window functions; m and o is scaling and translation parameters, respectively; the asterisk refers to an application window of the mother wavelet function; and $1/|m|^{1/2}$ is a normalization factor. Applying o and m equal 2^k, the signal is decomposed into its k levels constituent sub-signals: detail (d_i) and approximation (a_k) sub-signals. The orignal signals x(n) are converted to x′(n) through decomposition and reconstruction. The reconstruction signals x′(n) are linear superposition of the sub-signals:

$$x'(n)=\sum_{i=1}^{k}d_i+a_k \tag{7}$$

Decomposition errors Err between the original signals x(n) and the reconstruction signals x′(n) are defined as,

$$Err=\frac{1}{N}\sum_{k=1}^{N}|x(k)-x'(k)| \tag{8}$$

The decomposition errors Err are everaged value, which can be used to calcuate the decomposition error for a different D2 function.

The energy of sub-signals can be defined as sum of energy of detail signals E_j^d and energy of approximation signals E_j^d:

$$E_k=\sum_{i=1}^{n}|x_i|^2=E_k^a+\sum_{j=1}^{k}E_j^d \tag{9}$$

The energy of approximation signals is:

$$E_k^a=\sum_{t=1}^{N}|a_k(t)|^2 \tag{10}$$

The energy of detail signals is:

$$E_j^d=\sum_{t=1}^{N}|d_j(t)|^2 \tag{11}$$

Using wavelet transform, signals can be decomposed to multi-resolution. Further, macro-scale, meso-scale and micro-scale information of fluid dynamics can be obtained by Hurst exponent analysis of the sub-signals. Rescales range analysis (R/S analysis) is a powerful tool for calculating the Hurst exponent.

The one dimension time series x(n), with a length of N, decomposes into a series of n×b matrix when the value of n was selected as N/2, N/4, N/6--- and the corresponding value of b are 2, 4, 6---. For a chosen matrix, the cumulative deviation of the i element in the j column vector is calculated:

$$x_j(i) = \sum_{t=1}^{i} (x_j(t) - \bar{x}_j) \quad 1 \le i \le n, \quad 1 \le j \le b \tag{12}$$

where, the average $\bar{x}_j$ is:

$$\bar{x}_j = \frac{1}{n} \sum_{i=1}^{n} x_j(i) \tag{13}$$

The range function R(n) are determined as the maximum and minimum differences of time series $x_j(i)$ in each time interval, j:

$$R(j) = \max(x_j(i)) - \min(x_j(i)) \tag{14}$$

The standard deviation S(j) is:

$$S(j) = \sqrt{\frac{1}{n} \sum_{i=1}^{n} (x_j(i) - x_j)} \tag{15}$$

The R/S function is:

$$\left. \frac{R}{S} \right|_j = \frac{R(j)}{S(j)} \tag{16}$$

An empirical power law between expectation of R/S and time window n is applied to determine the Hurst exponent:

$$Ep\left(\frac{R}{S}\right)_n \propto n^h \tag{17}$$

In Eq. (17), Ep is the expectation function. When Hurst exponent h is equal to 0.5, the signals are totally stochastic series. When Hurst exponent bellows 0.5, the signals are rough anti-correlated series. When Hurst exponent is greater than 0.5, the signals are positively correlated series, which is known as a persistence one. Hurst exponent can be estimated by a linear regression of log(R/S) vs. log(n).